Form Approved
OMB No. 0704-0188

1. AGENCY USE ONLY (Leave blank)

2. REPORT DATE: 2/25/94

3. REPORT TYPE AND DATES COVERED: Technical 06/01/93 - 05/31/94

4. TITLE AND SUBTITLE
Atomic Force Microscopy of the Nacreous Layer in Mollusc Shells

5. FUNDING NUMBERS
N00014-90-J-1159

6. AUTHOR(S)
S. Manne, C. M. Zaremba, R. Giles, L. Huggins, D. E. Morse, G. D. Stucky, J. M. Didymus, S. Mann and P. K. Hansma

7. PERFORMING ORGANIZATION NAME(S) AND ADDRESS(ES)
University of California
Department of Chemistry
Santa Barbara, CA 93106

8. PERFORMING ORGANIZATION REPORT NUMBER
T12

9. SPONSORING/MONITORING AGENCY NAME(S) AND ADDRESS(ES)
Office of Naval Research
Chemistry Program
800 N. Quincy Street
Alexandria, VA 22217

10. SPONSORING/MONITORING AGENCY REPORT NUMBER

11. SUPPLEMENTARY NOTES
Prepared for Publication in The Royal Society Proceedings & Transactions B

12a. DISTRIBUTION/AVAILABILITY STATEMENT
Approved for public release;
distribution unlimited

13. ABSTRACT (Maximum 200 words)

We present atomic force microscopy observations of mature nacre, specifically the polygonal aragonite tablets which comprise the mineral portion of nacre, in two types of molluscs, a bivalve (*Atrina serrate*) and a gastropod (*Haliotis rufescens*). By imaging in liquids it was possible to dissolve away the nacre layer by layer to reveal both the structure of a single tablet and its relationship to vertically adjacent tablets. *Atrina* tablets (inner face) had a concave appearance; the central depression was surrounded by elongate rings mimicking the orientation and aspect ratio of the unit cell rectangle. Unit cell orientations were generally aligned vertically and laterally between tablets of *Atrina*, although occasional twinning was also observed. Etching (with HCl) initially removed a top "crust" in bleached *Atrina* tablets, revealing a flatter base without the elongate rings. Further etching lifted off individual tablets to reveal underlying nacreous layers, showing no morphological registry between vertically adjacent tablets. The nacreous structure of *Haliotis* differed from *Atrina* in three ways: 1)the tablets were flatter and showed no top "crust" or elongate rings; 2)the positions of the central depressions approximately repeated between nacreous layers, showing that the (presumed) nucleation sites line up along a given stack; and 3)the unit cell orientations were not preserved between laterally adjacent tablets but were between vertically adjacent tablets--an observation which could not be made by X-ray crystallography.

14. SUBJECT TERMS

15. NUMBER OF PAGES: 31

16. PRICE CODE

17. SECURITY CLASSIFICATION OF REPORT	18. SECURITY CLASSIFICATION OF THIS PAGE	19. SECURITY CLASSIFICATION OF ABSTRACT	20. LIMITATION OF ABSTRACT
Unclassified	Unclassified	Unclassified	UL

NSN 7540-01-280-5500

Standard Form 298 (Rev 2-89)
Prescribed by ANSI Std 239-18
298-102

DISCLAIMER NOTICE

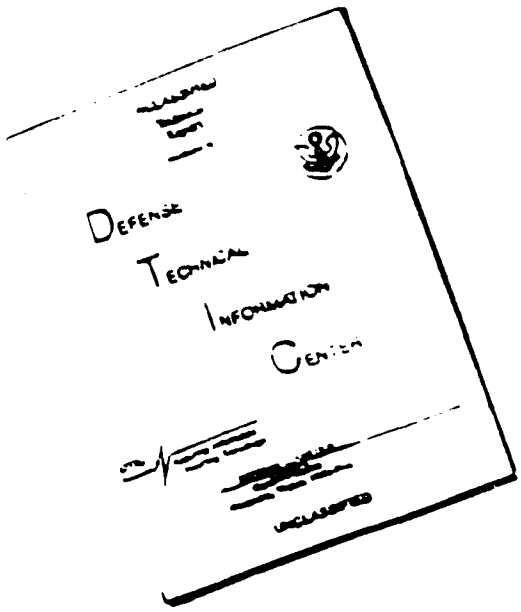

THIS DOCUMENT IS BEST QUALITY AVAILABLE. THE COPY FURNISHED TO DTIC CONTAINED A SIGNIFICANT NUMBER OF PAGES WHICH DO NOT REPRODUCE LEGIBLY.

OFFICE OF NAVAL RESEARCH

GRANT N00014-90-J-1159

R&T Code 413n007
Dr. John C. Pazik

Technical Report No.T12

Atomic Force Microscopy of the Nacreous Layer in Mollusc Shells

by

S. Manne, C. M. Zaremba, R. Giles, L. Huggins, D. E. Morse, G. D. Stucky,
J. M. Didymus, S. Mann, and P. K. Hansma

Prepared for Publication

in the

Royal Society Proceedings and Transactions B

University of California, Santa Barbara
Department of Chemistry
Santa Barbara CA 93106-9510

February 25, 1994

Atomic force microscopy of the nacreous layer in mollusc shells

S. Manne*[a], C.M. Zaremba[b], R. Giles[a], L. Huggins[c], D.E. Morse[c], G.D. Stucky[b], J.M. Didymus[d], S. Mann[d], and P.K. Hansma[a]

[a] Department of Physics
[b] Department of Chemistry
[c] Department of Marine Science
University of California, Santa Barbara, CA 93117 (USA)

[d] School of Chemistry, University of Bath, Claverton Down Bath BA2 7AY (UK)

We present atomic force microscopy (AFM) observations of mature nacre, specifically the polygonal aragonite tablets which comprise the mineral portion of nacre, in two types of molluscs, a bivalve (*Atrina serrata*) and a gastropod (*Haliotis rufescens*). By imaging in liquids it was possible to dissolve away the nacre layer by layer to reveal both the structure of a single tablet and its relationship to vertically adjacent tablets. *Atrina* tablets (inner face) had a concave appearance; the central depression was surrounded by elongate rings that mimicked the orientation and aspect ratio of the unit cell rectangle. Unit cell orientations were generally aligned vertically and laterally between tablets of *Atrina*, although occasional twinning was also observed. Etching (with HCl) initially removed a top "crust" in bleached *Atrina* tablets, revealing a flatter base without the elongate rings. Further etching of bleached samples lifted off individual tablets to reveal underlying nacreous layers, showing no morphological registry between vertically adjacent tablets. The nacreous structure of *Haliotis* differed from *Atrina* in three ways: 1) The tablets were flatter and showed no top "crust" or elongate rings; 2) the positions of the central depressions approximately repeated between nacreous layers, showing that the (presumed) nucleation sites line up along a given stack: and 3) the unit cell orientations (revealed by preferential etching) were not preserved between laterally adjacent tablets but *were* preserved between vertically adjacent tablets--an observation which could not be made by X-ray crystallography.

INTRODUCTION

The structure of the nacreous or pearly layer of mollusc shells has been an active area of research for several decades, resulting in hundreds of research papers [for reviews see (*1-5*)]. The principal techniques used have been scanning electron microscopy (SEM), transmission electron microscopy (TEM) and X-ray diffractometry (XRD). Previous work includes SEM images of a variety of mollusc shells (*3,6,7*); SEM and TEM of growth surfaces in bivalves (*8-11*) and in gastropods (*12,13*); and XRD of bivalve and gastropod nacre (*3,14*).

From these studies and many others, the emerging picture of nacreous architecture can be summarized as follows. Mature nacre consists of layers of aragonite ($CaCO_3$) tablets ("bricks") separated by organic macromolecules ("mortar"). The organics comprise only a few percent of the shell mass; they are thought to provide either a template for the nucleation of aragonite, or a preformed framework in which the mineral grows, or both. The thickness of nacreous layers is relatively uniform (0.5-1 μm), whereas the lateral size of the tablets (nominally 10 μm) can vary over an order of magnitude even in the same nacreous layer. Aragonite is oriented with its *c* axis normal to the nacreous layers. In bivalves the *a* and *b* axes are additionally well aligned between tablets of the same nacreous layer as well as between different nacreous layers, so that XRD perceives the entire nacreous region as approximately a single crystal. In gastropods, however, the *a* and *b* axes are randomly aligned. The growth surfaces of the nacre (the incompletely mineralized portions directly adjacent to the mantle tissue) also differ between these two classes of molluscs. In bivalves only the layer immediately adjacent to the growth solution contains small isolated tablets, implying that lateral growth and merging of tablets is rapid once nucleation has taken place. In gastropods, however, several layers adjacent to the growth solution contain

isolated tablets, with tablet size increasing progressively into the shell; the immature nacre thus resembles conical stacks of coins. This implies that lateral growth rate of tablets is comparable to vertical growth rate (i.e., nucleation rate of new tablets) in gastropods.

Despite these impressive results, electron microscopy of nacre is generally limited to static images of a single surface. It is not possible to image nacre in situ during a dissolution process, for example, which might reveal the structure of individual tablets or the relationship between tablets in adjacent nacreous layers. Such in situ imaging is possible with the atomic force microscope (AFM) (*15-17*). The AFM has already imaged biomineralized structures such as diatom shells (*18*), rat and human teeth (*19*), and matrix proteins of oyster shells (*20,21*). It has also imaged dynamic processes (in situ) on the surfaces of various biominerals; examples include pure crystal growth and dissolution of the biominerals calcite (*22,23*), fluorite (*24*) and hydroxyapatite (*19*), as well as modification of calcite growth in the presence of polyamino acids (*21*) and inorganic poisons (*25,26*). Here we present AFM results of mature bivalve (*Atrina serrata*) and gastropod (*Haliotis rufescens*) nacre during dissolution and compare these to earlier electron microscopy and X-ray crystallography studies.

EXPERIMENTAL

Atrina serrata was kindly provided by Prof. S. Weiner at the Weizmann Institute of Science, Israel. *Haliotis rufescens* was collected from the Pacific coast near Santa Barbara, CA. Mature nacreous layers were exposed for imaging either by mechanical cleaving or by bleaching. In the first case, a scalpel was wedged into a naturally existing space between nacreous layers, and these layers were pried apart by leverage. In the second case, nacre was stored in NaOCl (5% available chlorine) at

room temperature, which dissolved organic proteins and split the nacre into several planar pieces (washed with distilled water before imaging). Samples (typically 1 x 2 x 0.1 mm) were attached to stainless steel mounts using epikot resin. No further sample preparation was necessary.

We used a commercial AFM (*27*) operating in contact mode, with a 200 μm long, 36 μm wide triangular cantilever with an integrated oxide-etched tip (*27*). Imaging times were typically 30 s; imaging forces were typically 100 nN in air and 1-10 nN in liquid, though dissolving nacre in liquid was occasionally scanned at deliberately high forces (~100 nN) to induce tablet removal (see below). Fluid flow rate was adjusted via gravity feed and stopcock to around 5 μl/s, corresponding to a complete change of fluid cell volume every few seconds. All images shown are raw data unless indicated otherwise in the figure captions.

RESULTS

Bivalve (*Atrina serrata*)

Fig. 1 shows an AFM large scan of the inner face (facing the animal) of cleaved *Atrina* nacre in air. Three distinct nacreous layers are in evidence, around 0.6 μm thick, and each nacreous layer is composed of polygonal tablets of order 10 μm across. These tablets are concave on this face and have a small central dip: conversely AFM images of the outer face (facing the ocean) of *Atrina* nacre show convex tablets with a small central bump. The tablet concavity is consistent with SEM observations of the bivalves *Mytilus edulis* (growth surface) (*6,11*) and *Elliptio complanatus* (*5*), although small tablets on growth surfaces of bivalves can be convex (*8*). The depth of a concave tablet in Fig. 1, from boundary ridge to central depression, is typically 500 nm--small in

comparison to the lateral dimension of order 10 μm. (See Fig. 7 for a cross section of an *Atrina* tablet.) The thickness of the nacreous layer varies from 400 to 700 nm, depending on where the measurement is taken; this variation is typical of SEM observations of bivalve nacre (*8*). Evidently tablet concavity results both from increase of tablet thickness away from the center and from overall curvature of the tablet.

In addition to concavity, concentric elongate rings around the central dip are visible in most of the tablets (Fig. 1B). Wise observed similar rings in SEM images of *Mytilus* and *Pinna carnea* and speculated that they may be due to a daily cycle of mineral deposition (*3*). The AFM shows such rings in virtually all samples (bleached and unbleached) of *Atrina* tested, and two consistent features are worth noting. First, the orientation and size of the rings mimic those of the unit cell rectangle of the aragonite (001) plane; the short and long axes of the rings are parallel to the short and long (*a* and *b*) axes of the unit cell respectively, and the aspect ratio of the rings is around 5:8 as with the unit cell (*a*:*b* = 0.495:0.796 nm). (This observation is a result of comparing ring orientations to preferred etch directions, which in turn are compared to the tablet lattice imaged by AFM, discussed below.) Second, the ring orientations are well aligned both within one nacreous layer and between layers, consistent with X-ray data showing good alignment of aragonite crystals in bivalves (*3*).

Fig. 2 shows an etch sequence of bleached *Atrina* nacre (inner face) under flowing dilute HCl (*28*). The initial surface (Fig. 2A) is quite similar to that of the cleaved nacre (Fig. 1), showing concave tablets with central dips and surrounding nearly-rectangular rings, except that small bumps are visible primarily on the tablet boundaries (discussed below). The etch sequence of a nacreous layer proceeds as follows. First, the small bumps disappear almost immediately and the tablet begins to roughen (Fig. 2B). Second, a top "crust" (about 100 nm thick) begins dissolving off the tablet (Fig. 2C),

revealing a tablet "base" which shows distinct parallel rows (etch figures) parallel to the short axis of the original rings (i.e., the crystallographic *a* axis). Third, the top crust is almost completely removed from the imaging area (Fig. 2D). Note that a) the tablet boundaries are etched much faster than the interior, as evidenced by the deep cracks where there used to be ridges; b) the concavity of the tablet "bases" is far less than that of the original tablets; and c) the original concentric rings are no longer present, as though they were removed with the top crust. Note also that the tablet bases faithfully reproduce the lateral shape of the original tablet, showing that the same nacreous layer is still being imaged. Similar observations have been made by Mutvei on *Mytilus* and on *Nucula sulcata* (*29*).

As dissolution continues, tablets begin to abruptly lift off revealing the underlying nacreous layer (Fig. 2E). Probably tablets in adjacent layers are held together by a finite number of "anchor points," and liftoff occurs as a result of breaking the last anchor point either by dissolution, or force applied by the tip during scanning, or both. (The liftoff process can be speeded up by deliberately scanning at high force.) As more of the second nacreous layer is revealed (Fig. 2F), important morphological differences become apparent between this layer and the initial one. First, the tablet boundaries show cracks rather than ridges even when initially revealed. Second, the tablets show less concavity in the second nacreous layer. Third, elongate rings and parallel etch rows are far less pronounced and sometimes absent altogether. These differences indicate that the HCl is etching into underlying layers before they are exposed, via pores either pre-existing in the bleached sample or created by the etch itself. (For example, cracks created at tablet boundaries can provide solvent pathways into underlying nacreous layers.)

The exposure of underlying nacreous layers allows comparison of tablet "registry" between layers. Comparing Figs. 2B and 2F, it is apparent that neither the tablet shape nor its center position repeats in *Atrina*. Wada (*8*) has shown a correlation between the positions of tiny, growing tablets in a new nacreous layer and tablet boundary sites in the underlying mature layer, implying that nucleation is favored at tablet boundaries in bivalves. In our case nucleation sites of the mature tablets could not be identified, so this correlation could not be tested (*30*).

For the sample imaged in Fig. 2, the second nacreous layer also eventually lifted off revealing a third. However this did not repeat with the third nacreous layer. Tablets in this layer simply "etched down" (their thickness decreased continuously), and tablet boundaries widened until the fourth nacreous layer was visible through the cracks and only a thin film of the third nacreous layer was left. This different behavior may be due to the the limited penetration depth of the bleach into the nacre. The organic "mortar" was presumably dissolved or oxidatively removed from the first two interlayer spaces but not from the third, where it acted as an adhesive to bind the adjoining nacreous layers. In the first two interlayer spaces of the bleached sample, only mineralized bridges (unaffected by bleach) made contact between neighboring layers, and when these connections dissolved the tablets lifted off. There is ample electron microscopy evidence for such bridges between layers in bivalves (*8,10,29*).

When mechanically cleaved (unbleached) *Atrina* nacre was etched in the AFM, liftoff of tablets never occurred even in the first nacreous layer, giving further support to the above hypothesis. The top nacreous layer simply etched away as the images became more streaky (presumably due to contact between the tip and the acid-insoluble organic layer). Fig. 3 shows an etch sequence (in HCl) of a single triangular tablet from unbleached nacre. The initial tablet (3A) first roughens and develops boundary cracks

(3B); these cracks widen and the tablet etches down (3C) until only a thin film of the initial tablet is left (3D). The outline of the initial tablet is still evident after dissolution (3D), though the borders are wider and the thickness much smaller. Note that narrow, well-defined cracks appear inside the boundary of the initial tablet in Fig. 3D. The polygonality of these narrow cracks strongly suggests that they are tablet boundaries of the *underlying* nacreous layer, made visible through the remaining thin film of the top nacreous layer. This in turn suggests that underlying tablet boundaries protrude through the organic layer, forming mineralized bridges (revealed by HCl etch) to the top nacreous layer.

These mineralized bridges may serve as aragonite nucleation sites, explaining Wada's observation (*8*) that small tablets on the growth layer tend to be centered over tablet boundaries in the underlying layer. The small bumps observed on tablet boundaries in the bleached sample (Fig. 2A) might in fact be the bleach-insoluble (i.e., aragonite) parts of these bridges. These observations suggest that tablet boundaries are partially mineral, partially soluble organic matrix, and hence dissolve faster in HCl than the fully mineralized tablet interior.

AFM results also confirm XRD results on bivalve nacre. Fig. 4A is a closeup of an *Atrina* tablet during HCl etch, showing the preferential etch direction (arrow). Higher magnification (Fig. 4B) reveals the lattice on this surface, which is consistent with bulk termination of aragonite (001) (*31*); the lattice Fourier transform (inset) shows rectangular spots with spacing 0.5 x 0.8 nm, reproducing earlier AFM results with pressed nacre powder (*32*). Note that the lattice is better differentiated along the *b* axis (large spacing) than along the *a* axis (small spacing), giving the appearance of rows parallel to the *a* axis. Note also that the macroscopic row direction during etch (Fig. 4A) is along the *a* axis, as previously seen by SEM (*6*). Fig. 5A shows a twin boundary

on an *Atrina* tablet; the angle between etch rows is consistent with the nearly hexagonal (~120°) twinning along {110} observed in aragonite. The lattice resolution scan (Fig. 5B) clearly shows a corresponding abrupt change of lattice orientation.

Gastropod (*Haliotis rufescens*)

Fig. 6A shows an AFM image of bleached mature nacre of *Haliotis rufescens* which has been etched for 4 min in HCl. Like *Atrina*, *Haliotis* nacre is composed of polygonal tablets with central depressions; but unlike *Atrina*, the tablets are flat (not concave) and show no boundary ridges or elongate rings; see Fig. 7 for a comparison of cross sections. The dissolution process (in HCl, pH 3.3) of *Haliotis* nacre is similar to *Atrina* in that tablet boundaries initially widen until the tablet lifts off as a whole; however there is no evidence of a top crust in the first nacreous layer, as with *Atrina*. The etch highlights a certain direction on each tablet (Fig. 6A), assumed to be the *a* axis direction as with *Atrina*. Note however that these directions differ randomly from tablet to tablet in this layer, confirming the overall lack of *a* and *b* axis orientation observed in gastropods (*3*). Sometimes even on the same tablet there exist regions of differing orientations (see Fig. 6B), and the angle between these orientations is generally consistent with twinning.

Exposure of new nacreous layers by dissolution (Fig. 6) shows two important relationships which set *Haliotis* apart from *Atrina* (and gastropods apart from bivalves in general). First, though the tablet shapes are quite different between adjacent nacreous layers of *Haliotis*, the lateral positions of the central depressions are always approximately the same (to within about 0.5 μm) (*33*). This observation is consistent with TEM images of vertical cross sections (*13*). Second, in *Haliotis* tablets where the *a* axis (etch direction) is readily identifiable, this direction approximately repeats (to within

~10°) in the underlying tablet. In other words, the *a* and *b* axes are well aligned vertically through the shell but not laterally. (For tablets which are twinned, one of the twin directions repeats in the next nacreous layer.) Although this interlayer alignment was suspected from uniformly elongated coin stacks in some gastropods (*3*), confirmation by X-ray crystallography was not possible due to the small lateral area of this alignment. The AFM confirms, by etching successive nacreous layers, that such vertical alignment exists.

DISCUSSION

The structural differences observed between *Atrina* and *Haliotis* nacre could reflect distinct biomineralization strategies. The curvature of *Atrina* tablets could be induced by the juxtaposition of crystals and epithelial cells at the interface with the extrapallial fluid. Since the growth front in bivalve nacre proceeds at a rate that permits extensive lateral development of individual crystals, a replica of each apposed cell could be established in the inorganic growth morphology. Moreover, the distinct crust observed in bivalve nacre may be due to occlusion of cellular products into the crystal surface adjacent to the epithelial cells. In gastropods, by contrast, the production of new layers rather than extended intralayer lateral growth suggests a relatively fast rate of cell withdrawal from the growth front. The absence of apposed cells during lateral growth of the tablet would account for both the flat crystal surface and the lack of a top crust in gastropods.

Dissolution of unbleached *Atrina* nacre showed evidence for mineralized connections between two nacreous layers, originating at tablet boundaries in the underlying nacreous layer. These observations suggest that the vertical crystallographic alignment of bivalve nacre is a consequence of crystallographic continuity between

layers rather than episodic nucleation on newly secreted organic templates. The staggered vertical arrangement of crystals provides an organizational structure in which adjacent intralayer tablets can also be crystallographically contiguous through mineral bridges to a common underlying crystal. In this regard, it is conceivable that the long range crystallographic order is achieved by one (or a few) nucleation site(s) in the first layer of the nacreous architecture. The long range alignment of the *a* and *b* directions could be attained, not by epitaxial recognition at the surface of the organic matrix, but by the coherent intergrowth of adjacent crystals via the mineralized bridges that are presumably produced by pores in the organic framework.

In contrast the *Haliotis* tablets show no lateral alignment of the *a* and *b* axes within a given layer, but do show that the tablets are crystallographically coherent within individual stacks. This suggests that each stack represents an individual nucleation center that induces preferential orientation of the crystallographic *c* axis. Although mineralized connections were not observed by AFM between the intrastack crystals, it is possible that such connections exist, perhaps within the central region of each tablet.

CONCLUSION

The AFM results presented in this paper confirm and extend previous SEM, TEM, and XRD studies of the nacreous layers of molluscan shells. In particular, our studies of native and treated samples have highlighted significant morphological and structural differences between bivalve (*Atrina serrata*) and gastropod (*Haliotis rufescens*) nacre that may reflect different biomineralization strategies. In both organisms, the individual aragonite tablets are oriented with the *c* axis perpendicular to the nacre plane, exhibit central depressions (elevations) on the inner (outer) face, and show preferential etching along the *a* axis in the presence of HCl. However, *Atrina* nacre consists of

tablets that show a concave inner face which exhibits a distinct texture (crust) and crystallographically-oriented rings, while the *Haliotis* tablets are flat and uniform. Moreover, *Atrina* nacre is crystallographically coherent both within and between layers, whereas *Haliotis* nacre shows interlayer but no intralayer registry of the *a* and *b* axes.

REFERENCES

1. H.A. Lowenstam and S. Weiner, *On Biomineralization*. Oxford University Press, New York 1989.

2. S. Weiner, *CRC Crit. Rev. Biochem.* **20**, 365 (1986).

3. S.W. Wise, *Eclogae geol. Helv.* **63**, 775 (1970).

4. N. Watabe, *Prog. Crystal Growth Charact.* **4**, 99 (1981).

5. K.M. Towe, *Biomineralization* **4**, 1 (1972).

6. H. Mutvei, *Biomineralization* **2**, 48 (1970).

7. H.K. Erben, *Biomineralization* **4**, 15 (1972).

8. K. Wada, *Biomineralization* **6**, 141 (1972).

9. K.M. Towe and G.H. Hamilton, *Calc. Tiss. Res.* **1**, 306 (1968).

10. G. Bevelander and H. Nakahara, *Calc. Tiss. Res.* **3**, 84 (1969).

11. H. Mutvei, *Calcif. Tiss. Res.* **24**, 11 (1977).

12. S.W. Wise and W.W. Hay. *Trans. Amer. Microsc. Soc.* **87**, 419 (1968).

13. H. Nakahara, in *Mechanisms and Phylogeny of Mineralization in Biological Systems*, S. Suga and H. Nakahara, Eds. Springer-Verlag, Tokyo 1991, p. 343.

14. K. Wada, *Bull. Natl. Pearl Res. Lab. Japan* **7**, 703 (1961).

15. G. Binnig, C.F. Quate and Ch. Gerber, *Phys. Rev. Lett.* **56**, 930 (1986).

16. D. Rugar and P.K. Hansma, *Physics Today* **43**, 23 (October 1990).

17. D. Sarid, *Scanning Force Microscopy: With Applications to Electric, Magnetic, and Atomic Forces.* Oxford University Press, New York 1991.

18. A. Linder, J. Colchero, H.-J. Apell, O. Marti and J. Mlynek, *Ultramicroscopy* **42-44**, 329 (1992).

19. S. Kasas, A. Berdal and M.R. Celio, *Scanning Probe Microscopies II*, C.C. Williams, Ed., Proc. SPIE **1855**, 17 (1993).

20. J.E. Donachy, B. Drake and C.S. Sikes, *Marine Biology* **114**, 423 (1992).

21. A. Wierzbicki, C.S. Sikes, J.D. Madura and B. Drake, *Calc. Tiss. Internat.* (in press).

22. A.J. Gratz, P.E. Hillner and P.K. Hansma, *Geochim. Cosmochim Acta* **57**, 491 (1993).

23. P.E. Hillner, A.J. Gratz, S. Manne and P.K. Hansma, *Geology* **20**, 359 (1992).

24. P.E. Hillner, S. Manne, A.J. Gratz and P.K. Hansma, *Faraday Discussions* 95 (in press).

25. A.J. Gratz and P.E. Hillner, *Journal of Crystal Growth* 129, 789 (1993).

26. P.M. Dove and M.F. Hochella Jr., *Geochim. Cosmochim. Acta* 57, 705 (1993).

27. Digital Instruments, Santa Barbara, CA.

28. The pH of the flowing HCl solution was kept between 3 and 4 for etch experiments. In this range the etch process was slow enough to be followed by the AFM.

29. H. Mutvei, *Scanning Electron Microscopy* 2, 457 (1979).

30. We cannot assume that the central depressions of *Atrina* tablets are the original nucleation sites of these tablets, as seems to be the case in gastropods (*13*). The overall shape of the top crust (the concavity and the central depression) might be due to intimate contact between epithelial cells and partially grown tablets.

31. The area on which the (001) plane could be resolved on an asperity was quite small, typically no more than 10 x 10 nm (as in Fig. 4B). Sometimes other periodicities not corresponding to the (001) plane could also be resolved; these may be due to higher-index planes on the steep walls of the asperities.

32. G. Friedbacher, P.K. Hansma, E. Ramli and G.D. Stucky, *Science* **253**, 1261 (1991).

33. The reader can confirm this by placing a transparency over Fig. 6A, tracing the image square and marking the position of each central depression, then overlaying this transparency on each of the following layers (Figs. 6B-D). Other than a slight offset caused by sample motion, the centers line up within ~0.5 μm.

34. We thank D. Walters, A. Beltcher and P.E. Hillner for useful discussions. This work was supported by the National Science Foundation, Office of Naval Research, Materials Research Laboratory grant, and an AT&T Fellowship (to S. Manne).

FIGURE CAPTIONS

Fig. 1: 38 x 38 μm topview images of cleaved *Atrina* nacre (inner face). A) Height mode image, with a z-range of 2.0 μm between black (lowest) and white (highest). B) Simultaneous error signal image, showing high-spatial-frequency information which is not compensated by the feedback loop; this image shows better lateral contrast, but the grey scale here is related to a spatial derivative (not height). Three nacreous layers are visible, as are polygonal aragonite tablets in two of the layers. The height image shows that these tablets are concave, with ridges along the boundaries and small depressions near the centers. The error signal image highlights the concentric elongate rings surrounding the central depression of each tablet.

Fig. 2: Time sequence of dissolution of bleached *Atrina* nacre in HCl. All images (topview, height mode) are 32 x 32 μm with a z-range of 1.2 μm; images B-F are of the same sample area. A) Initial nacre in air showing concave tablets with central depressions, elongate (nearly rectangular) rings, and small bumps on the tablet boundaries. B) Image in flowing HCl, t = 2 min after starting flow; note that bumps on tablet boundaries have disappeared, and tablets show signs of roughening. C) t = 9 min; tablets show increased roughening and a top crust begins to dissolve off. D) t = 13 min; top crust has virtually disappeared, revealing flatter tablet bases with pronounced parallel etch figures (nearly vertical rows) as well as an occasional twin boundary (arrow); note cracks indicating fast dissolution at tablet boundaries, and the disappearance of elongate rings. E) t = 19 min; whole tablets begin to lift off, revealing underlying nacreous layer. F) t = 26 min; more of the underlying layer is revealed, showing tablets with less pronounced topography (e.g., smaller concavity, fainter central depressions and fainter rings) than in the first layer.

Fig. 3: Time sequence of dissolution of unbleached *Atrina* nacre in HCl. All images (topview, height mode) are 21 x 21 μm with a z-range of 1.0 μm, and are taken from the same sample area. A) Image of a single tablet before dissolution. B) t = 9 min after start of dissolution; tablet is less concave, and etch cracks appear at the tablet boundary. C) t = 18 min; boundary cracks widen, top crust dissolves off, and very faint cracks (arrows) begin to appear inside the tablet boundaries. D) t = 22 min; only a thin film of the original triangular tablet is left, with the original outline still faintly visible; thin cracks inside tablet boundary are now prominent, perhaps revealing the location of mineralized interlayer bridges.

Fig. 4: Closeup of *Atrina* tablet after a few minutes of dissolution in HCl. A) Topview, height mode image, size 2.4 x 2.4 μm and z-range 250 nm, showing preferential etch direction (arrow). Note that etch rows are made up of discrete "tip images" caused by sharp asperities imaging the AFM tip rather than vice versa; a few larger tip images are also visible. [For a reference on tip images see P. Grütter, W. Zimmermann-Edling and D. Brodbeck, *Appl. Phys. Lett.* **60**, 2741 (1992).] B) Deflection mode image (lowpass filtered), size 20 x 20 nm, showing the lattice on this surface. Inset Fourier transform shows periodicities corresponding to a rectangular unit cell, size 0.45 x 0.80 nm (±10%), which is consistent with *c* axis aragonite. Note that the *a* axis (arrow) is parallel to the etch rows.

Fig. 5: Closeup of *Atrina* tablet showing a twin boundary. A) Topview, height mode image, size 1.2 x 1.2 μm and z-range 150 nm, showing the change in direction of the etch rows. B) Deflection mode image, size 28 x 28 nm, showing the same change in direction of the *a* axis rows at the twin boundary.

Fig. 6: Time sequence of dissolution of bleached *Haliotis* nacre in HCl (pH 3.3). All images (topview, height mode) are 12 x 12 μm with a z-range of 400 nm, and are taken from the same sample area. A) t = 4 min after start of dissolution, first nacreous layer; B) t = 30 min, second nacreous layer; C) t = 57 min, third nacreous layer; D) t = 89 min, fourth nacreous layer. In each layer, each tablet has a well-defined central depression and (usually) a well-defined etch direction, as indicated by arrows for the five tablets in the center of the image. Some tablets have more than one etch direction, indicating twin boundaries. Note that the position of the central depression approximately repeats from layer to layer, as does the etch direction (when identifiable), indicating crystallographic alignment in the vertical though not lateral direction. (Where there is a twin boundary, i.e., there are two etch directions associated with a given central depression, one of the two directions repeats in the underlying layer.)

Fig. 7: Cross sections across the inner face of typical *Atrina* (top) and *Haliotis* (bottom) tablets. Cross sections have the same lateral scales (7.5 μm from left to right, marked at intervals of 1 μm) and vertical scales (0.5 μm from top to bottom, marked at intervals of 0.1 μm). Heavy arrows denote tablet boundaries. The *Atrina* tablet is concave overall, but this concave slope is periodically interrupted by elongate rings (positions indicated by light arrows). The *Haliotis* tablet is much flatter but has a pronounced central depression.

FIGURE 1A

FIGURE 1B

FIGURE 2A

FIGURE 2B

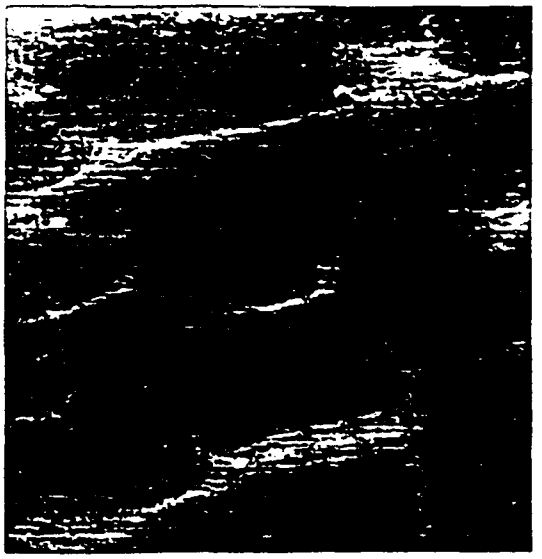

FIGURE 2C

FIGURE 2D

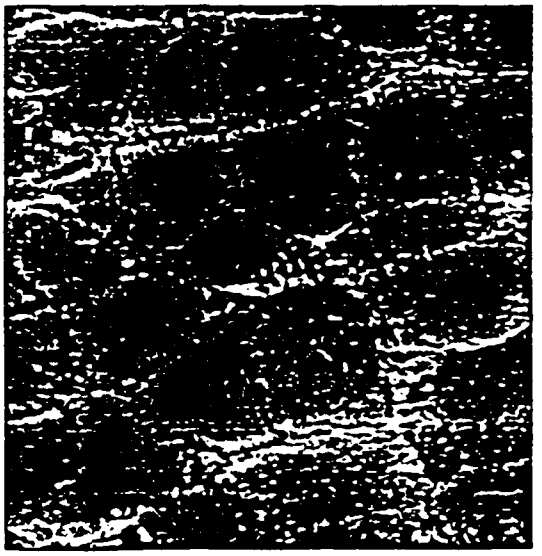

FIGURE 2E

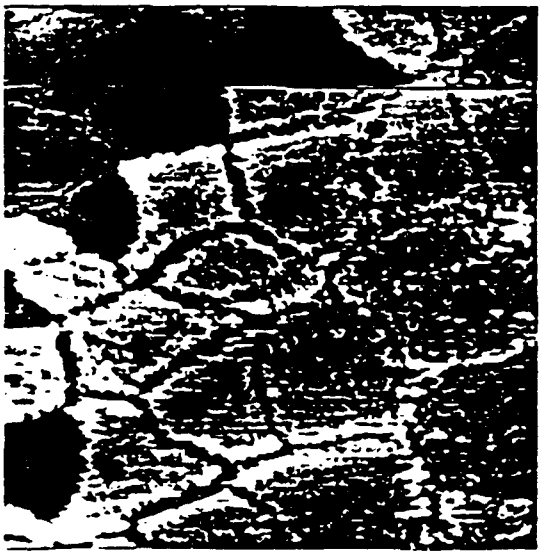

FIGURE 2F

FIGURE 3A

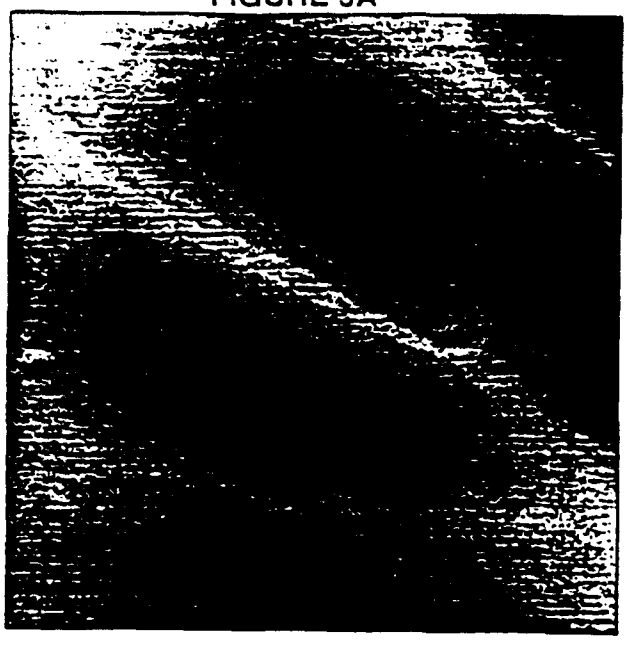

FIGURE 3B

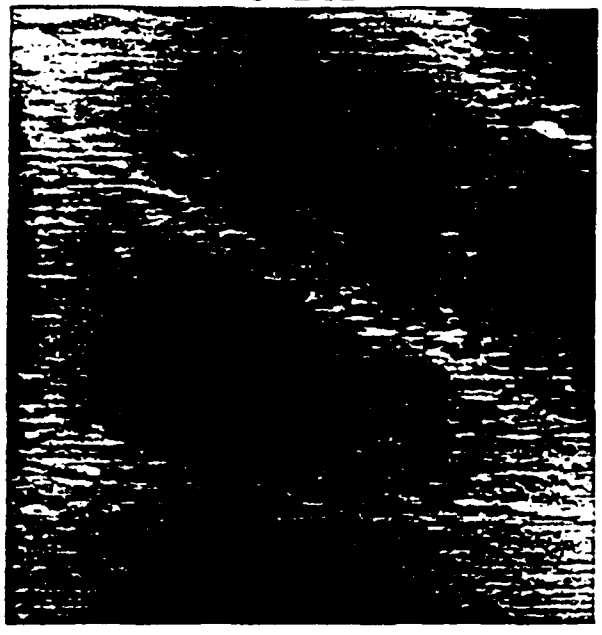

FIGURE 3C

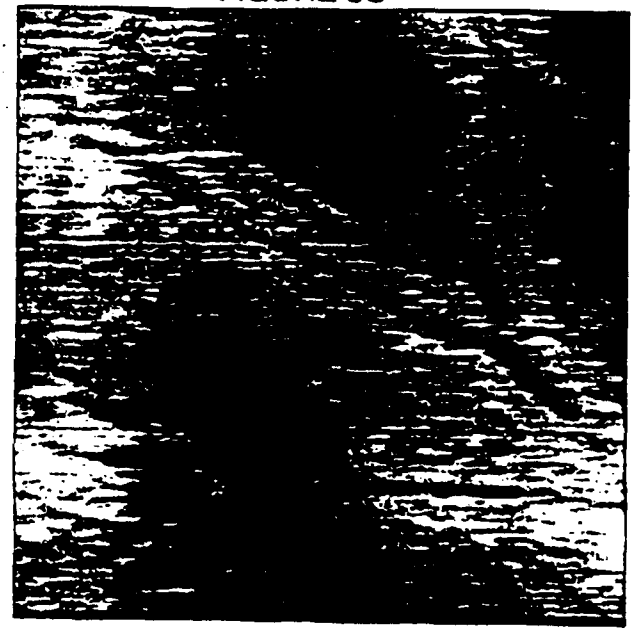

FIGURE 3D

FIGURE 4A

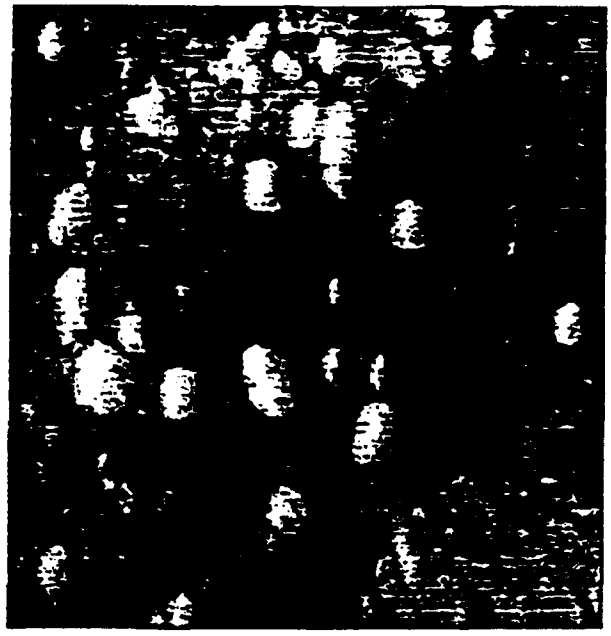

FIGURE 4B

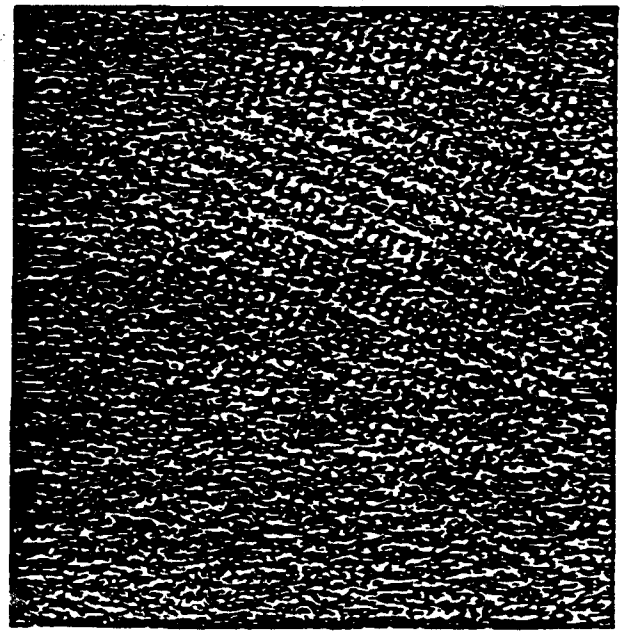

FIGURE 5A

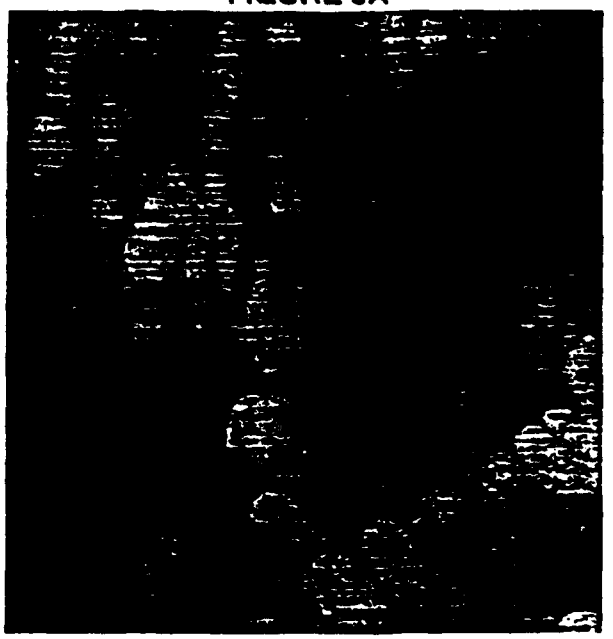

FIGURE 5B

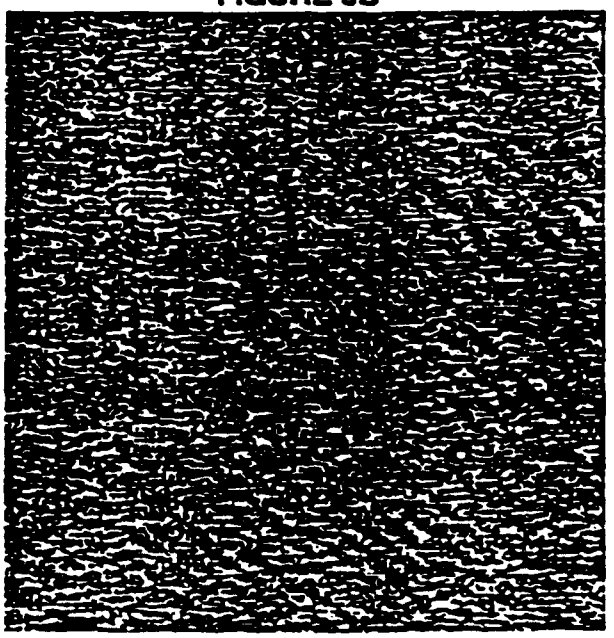

FIGURE 6A

FIGURE 6B

FIGURE 6C

FIGURE 6D

FIGURE 1A

FIGURE 1B

FIGURE 2A

FIGURE 2B

FIGURE 2C

FIGURE 2D

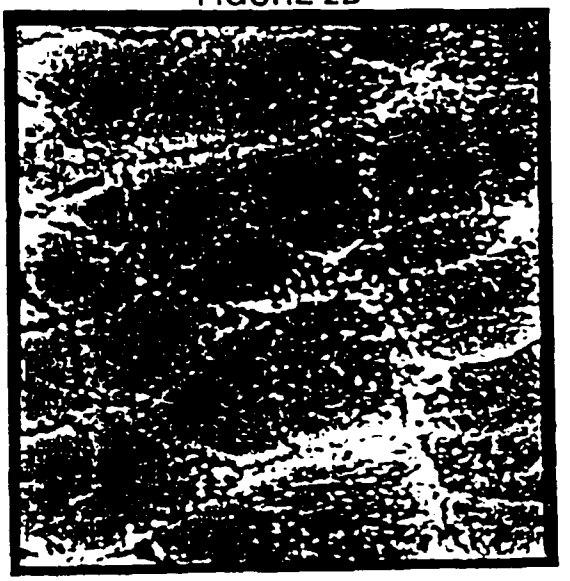

FIGURE 2E

FIGURE 2F

FIGURE 3A

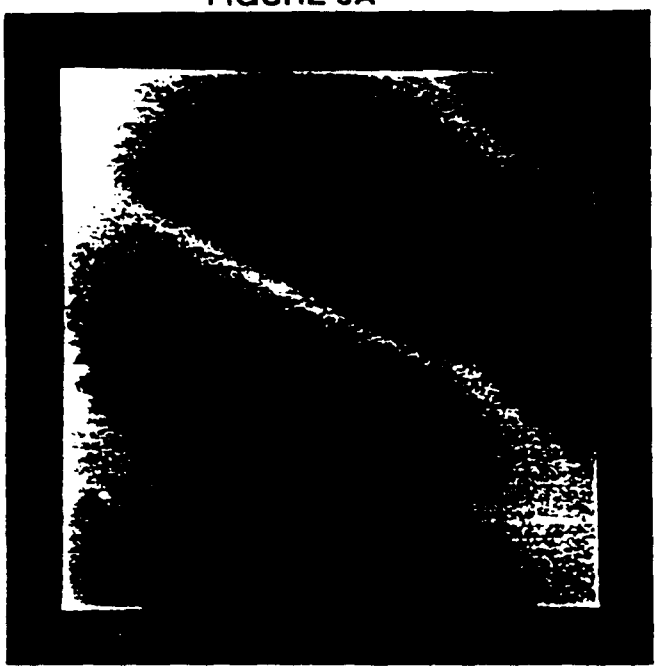

FIGURE 3B

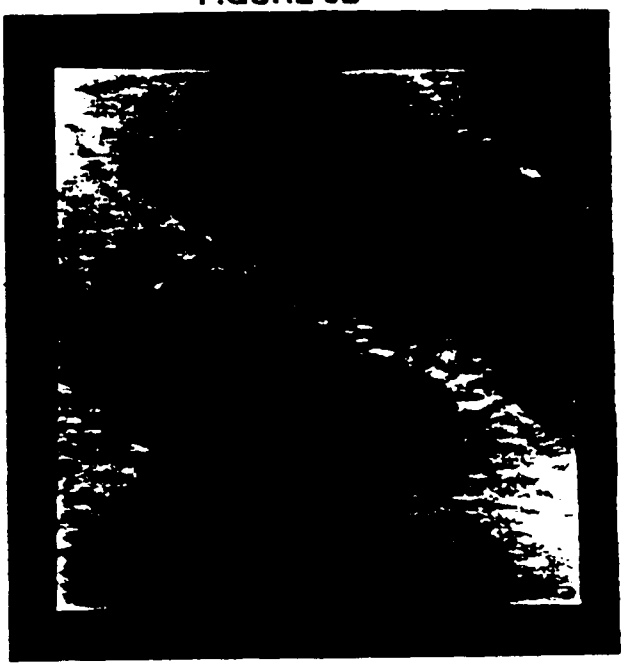

FIGURE 3C

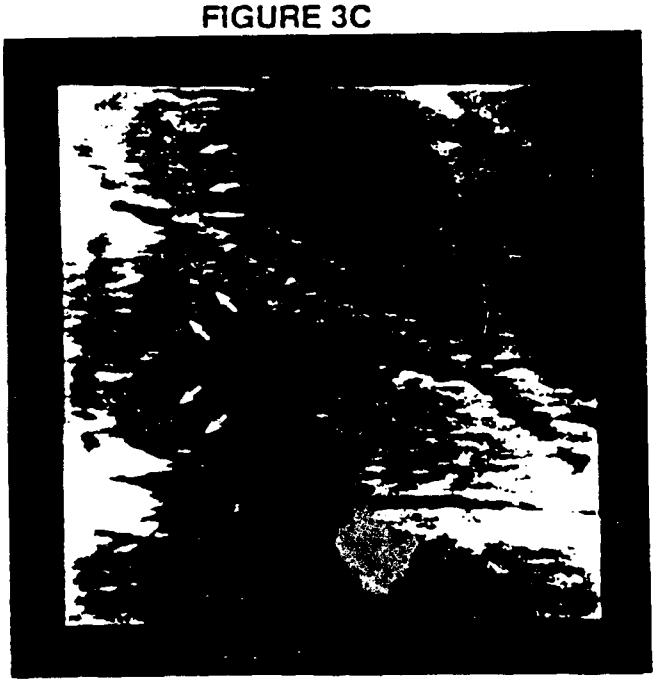

FIGURE 3D

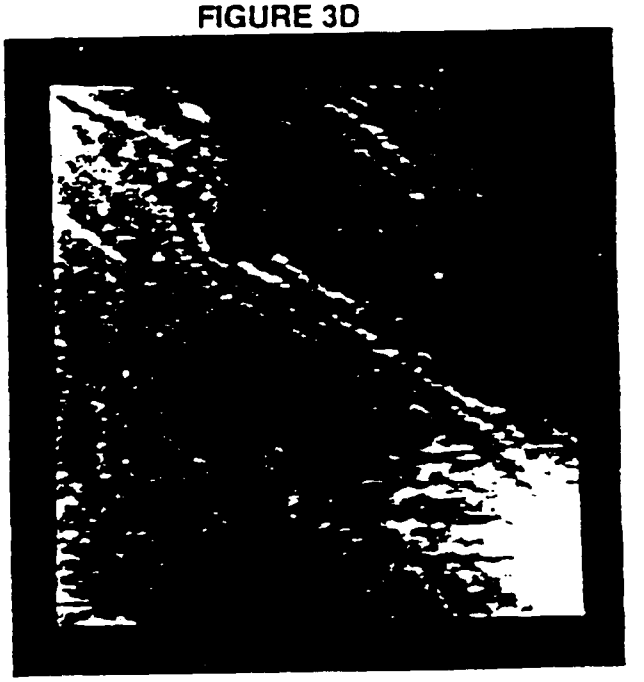

FIGURE 4A

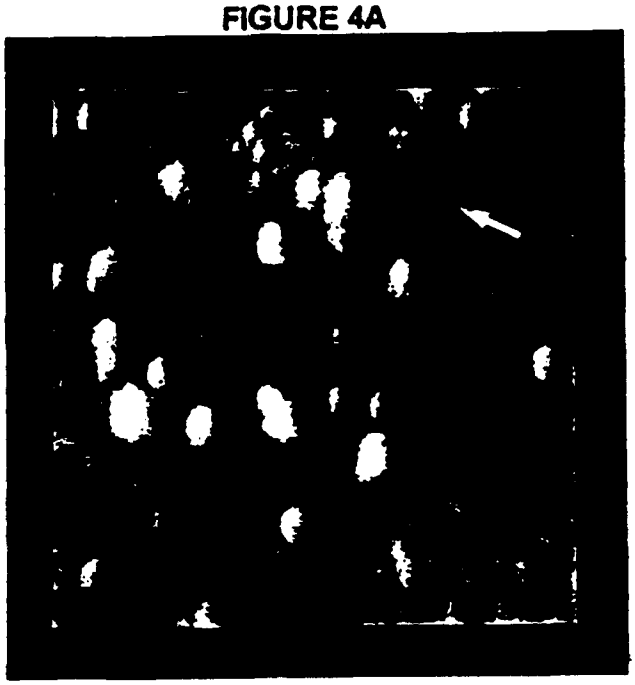

FIGURE 4B

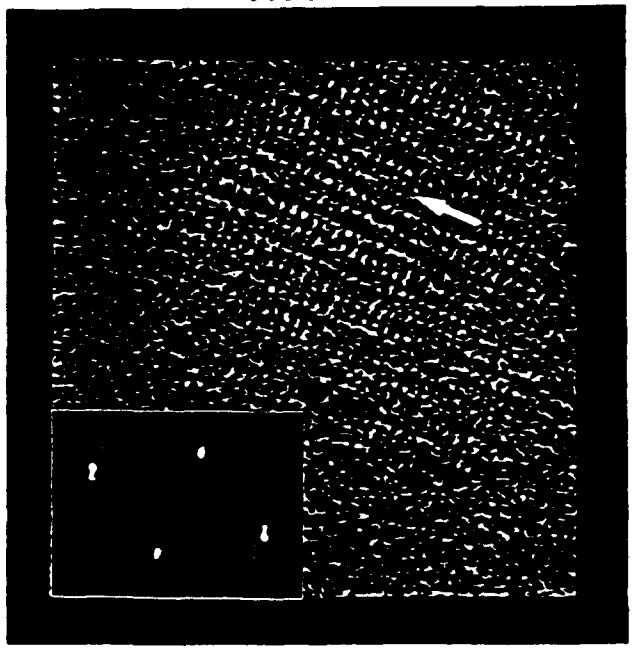

FIGURE 5A

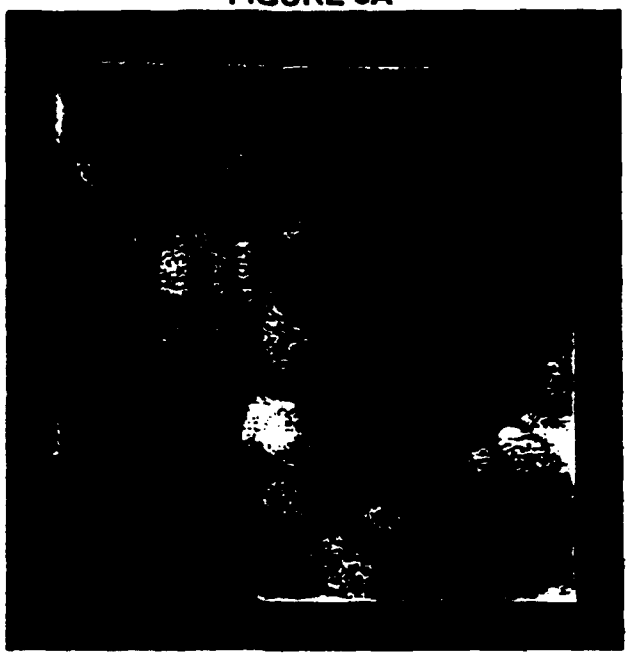

FIGURE 5B

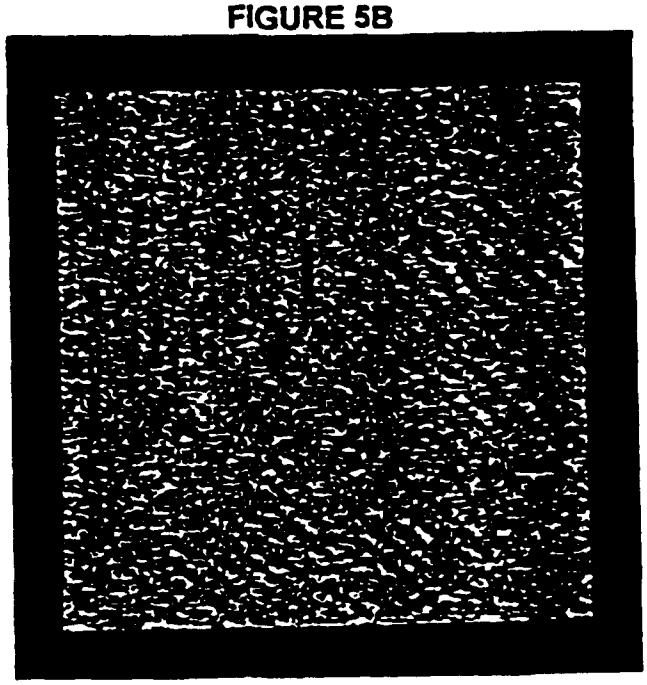

FIGURE 6A

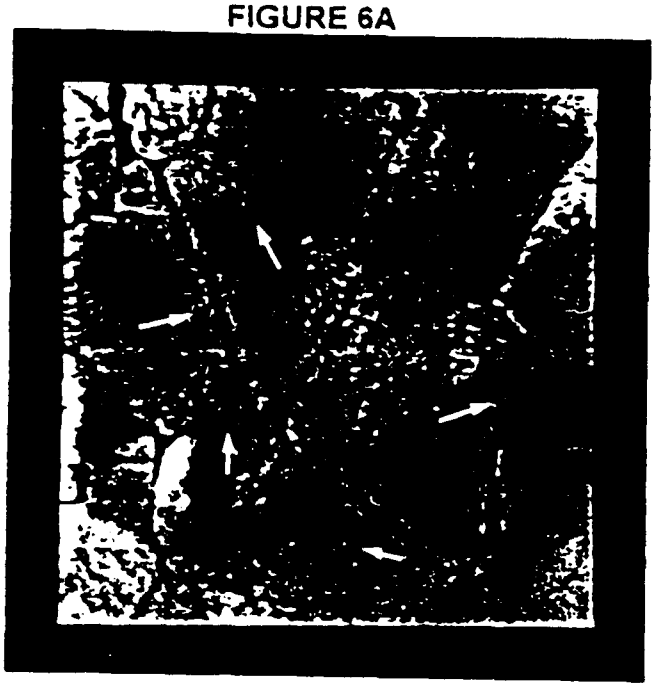

FIGURE 6B

FIGURE 6C

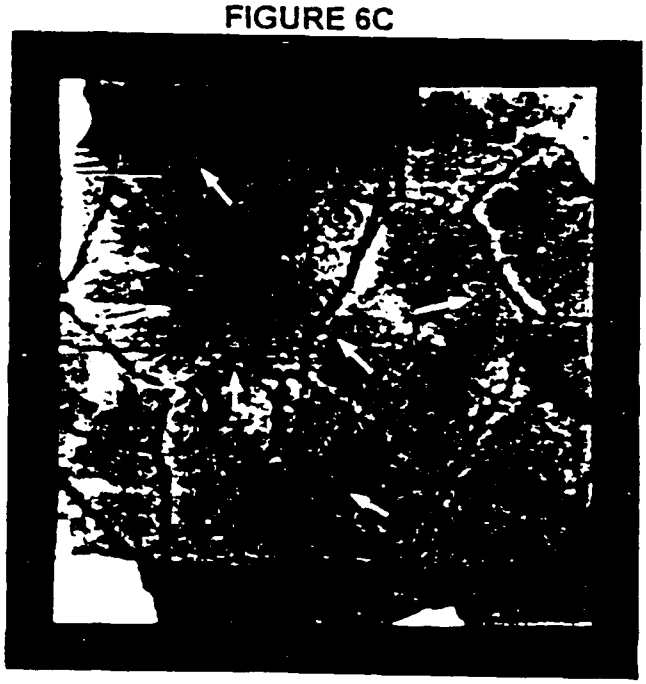

FIGURE 6D